Medical Image Segmentation by Fuzzy Logic Techniques

Yutaka Hata, Syoji Kobashi and Shoji Hirano

Department of Computer Engineering, Himeji Institute of Technology,
2167, Shosha, Himeji, 671-2201, Japan
hata@comp.eng.himeji-tech.ac.jp

ABSTRACT

This paper describes useful fuzzy logic techniques for medical image segmentation. Specific methods to be reviewed include fuzzy information granulation, fuzzy inference and fuzzy cluster identification. Fuzzy information granulation is introduced as a powerful scheme to find the thresholds to obtain the whole brain region in MR data. Fuzzy inference technique succeeds to segment the brain region into the left cerebral hemisphere, right cerebral hemisphere, cerebellum and brain stem. The fuzzy inference aided segmentation procedure is also useful to human foot CT image. Fuzzy cluster identification is adapted to determine the obtained clusters into blood vessel or other tissues in MRA image.

1. INTRODUCTION

In the medical field, automatic segmentation of the Region of Interest (ROI) is available to diagnose the human function[1]. Generally, image segmentation is a particularly critical problem owing to the complexity of the images. To deal with such the difficulty, a mixture of pattern recognition and fuzzy logic techniques leads to successful tasks to segmentation of the ROI and to give enhanced anatomical resolution[2]-[10]. Such fuzzy expert systems also have shown themselves to be a powerful framework for building knowledge systems.

This paper provides our medical image processing procedures. Specific methods to be reviewed include fuzzy information granulation(IG)[11], fuzzy inference[12]-[14] and fuzzy cluster identification. These fuzzy logic techniques will be able to demonstrate the medical knowledge. Fuzzy information granulation is explored as a threshold finding procedure to segment whole brain region in human brain MR data set[7][8]. Fuzzy information granulation is done by matching the intensity histogram with histogram models able to concentrate the various brain histograms. We can obtain the whole brain region on evaluating the obtained thresholds. The experimental results of the segmented brain volume comparison on 50 data sets show that the error ratio was 2.3 % on the average. For the obtained whole brain volumetric data, fuzzy inference technique employing intensity, location and boundary knowledge succeeds to segment it into the left cerebral hemisphere, right cerebral hemisphere, cerebellum and brain stem[9][10]. The experimental results on 36 data sets show that the error ratio was 2.5 % on the average. Moreover, fuzzy inference employing joint, intensity and boundary knowledge gives us a powerful segmentation procedure of human foot CT image to their ossa[9]. The experimental results on seven foot CT images show that a medical doctor reconfirms that five calanneri are correctly segmented and their articular facet can be clearly observed. Fuzzy cluster identification is applied to MRA image. After hierarchy clustering can classify all voxels in the image to some clusters, our fuzzy cluster identification is adapted to determine these clusters into blood vessel or other tissues. Consequently, all methods can produce good results that are satisfying to practical use for medical imaging.

2. THRESHOLD FINDING BY FUZZY INFORMATION GRANULATION

2.1 Preliminaries

We obtained the MR volumetric images from the Sigma Advantage 1.5 Tesla MRI Scanner (General Electric Inc.) using the circularity polarized head coil as both transmitter and receiver. The image acquisition method was coronal 3D SPoiled GRadient echo (SPGR) with TR = 14msec, TE = 3msec and flip angle = 20 degrees. Field of View was 220mm. Matrix was 256 by 256. Each of the volumes is made up of 124 separate slices whose thickness is 1.5mm. The dimension of giving voxel is $0.86 \times 0.86 \times 1.5 mm^3$. We construct the volumes of the human brain, which consisted of $124 \times 256 \times 256$ voxels. In our system, the feature images appear and are treated as intensity images. The intensity of all intracranial structure ranged between 0 and 255.

2.2 Threshold Finding by Fuzzy IG

Figure 1 shows a histogram of a human brain MR images. The histogram consists of the coherent gray levels of the CSF, gray matter, white matter and others. The intensity level of the others is smaller than one of the CSF. By understanding their peaks, we can find the required thresholds Th_1 and Th_2 as shown in Figure 1. We treat their peaks as the fuzzy granules. Figure 2 is an illustration of the histogram neighbor peak P. In this histogram, by differential calculus operating, we can extract three poles, p_1, p_2 and p_3, whose intensities are denoted by I_1, I_2 and I_3, respectively. The numbers of voxels at the poles are V_1, V_2 and V_3, respectively. We call the partial curve between p_1 and p_3, "peak." The granule (peak) is associated with the fuzzy attributes, *sharpness* and *magnitude* defined below,

0-7803-4778-1/98 $10.00 © 1998 IEEE

$$\text{sharpness}(P) = \frac{H}{W} = \frac{V_3 - \frac{V_1 + V_2}{2}}{I_3 - I_1}$$

and

$$\text{magnitude}(P) = \int_{I_1}^{I_3} v(i)di - N_t(P),$$

where $N_t(P) = \frac{(V_1 + V_2) \times (I_3 - I_1)}{2}$.

Each peak can be represented by fuzzy languages. The membership functions for the employed fuzzy languages are given in Figure 3. Thus the histogram is recognized as the collection of the peaks whose attributes are represented by the fuzzy languages. Figure 4 shows our histogram models, Model A and Model B, able to concentrate various histograms. Table 1 shows the knowledge representation of the models. We can derive the granules and can find two thresholds by comparing an input histogram with our histogram models by the following steps.

Table 1 Fuzzy membership functions of the models.

Granule	Histogram Model A		Histogram Model B	
	sharpness	*magnitude*	*sharpness*	*magnitude*
G_g	rather big	rather big	rather big	rather big
G_w	big	big	big	big
G_c	not exist	not exist	rather small	rather small

Step 1) Derive all possible patterns for evaluating which possibility, Model A or Model B, is higher for the input.

Step 2) For the each peak, compute *sharpness* and *magnitude*.

Step 3) Compute a minimum between *attribute* values, sharpness and magnitude, and the corresponding membership functions for each peak. We obtain the average values, A_s (for *sharpness*) and A_m (for *magnitude*). Similarity measure, $A_s + A_m$, is calculated. Pick up the pattern with the maximum similarity measure and employ the model that the pattern belongs to.

The interested histogram is thus classified into a model that has the maximum similarity measure. From the obtained peaks specifying the input histogram, we can obtain the required thresholds.

2.2 Experimental Result

We segment 50 human brain MR volumes by the obtained thresholds and calculate their volumes. The results are compared with the manually segmented ones by a medical doctor. The manually segmented results are obtained by tracing their outlines for every image slice of the MR volumes. The segmentation accuracy obtained by averaging the absolute values of error ratio was 2.3% for 50 MR volumes. The standard deviation was 0.22.

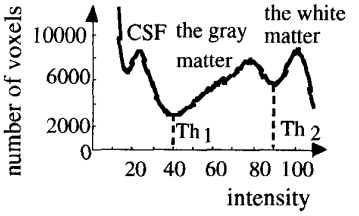

Figure 1 A histogram of brain MR image.

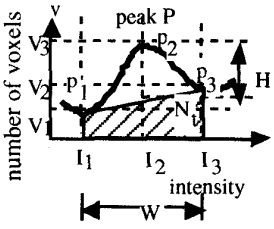

Figure 2 An Illustration.

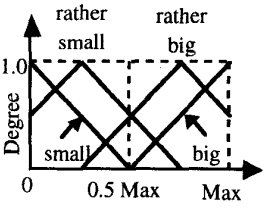

Figure 3 Membership functions

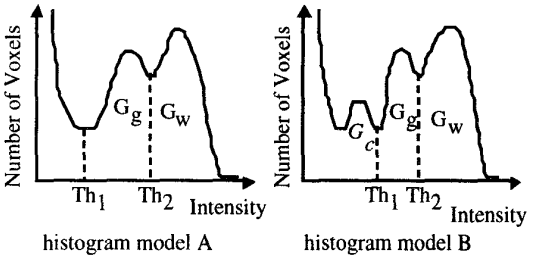

Figure 4 Two histogram models.

3. SEGMENTATION BY FUZZY INFERENCE

3.1 Fuzzy Inference on Image Segmentation

Image segmentation needs to help with human knowledge. We consider possible knowledge to segment the ROIs and we will represent the obtained information by fuzzy if-then rules. Consider to segment several ROIs in an image. We represent the entire knowledge residing within a collection of rules to segment the ROIs:

Knowledge 1:

If $x_{mn}=A_1$ then $x_{mn}=G_{11}$,

Else if $x_{mn}=A_2$ then $x_{mn}=G_{12}$, ...

Knowledge p: (p=2, 3, ...)

If $x_{mn}=C_1$ then $x_{mn}=G_{p1}$,

Else if $x_{mn}=C_2$ then $x_{mn}=G_{p2}$, ...

Note that the all rules are evaluated to achieve same goal: segmenting the ROIs. The membership values of G' are calculated by:

From Knowledge 1:

$$\mu^{1}_{G'}(x_{mn}) = \max_{m\times n\in M\times N} \min(\mu_{A'}(x_{mn}), \mu_R(x_{mn}, x_{mn})).$$

From Knowledge p (p=2, 3,...)

$$\mu^{p}_{G'}(x_{mn}) = \max_{m\times n\in M\times N} \min(\mu_{C'}(x_{mn}), \mu_R(x_{mn}, x_{mn})).$$

Next step is constructing the pixels to ROIs. We should effectively and selectively employ the inference results $\mu^{1}_{G'}(x_{mn}),\ldots,\mu^{p}_{G'}(x_{mn})$. The typical constructing techniques are known in labeling, region growing or clustering techniques.

3. 2 Application to MR and CT Images

3.2.1 Human Brain MR Images

Section 3.2.1 applies the image segmentation to MR brain images. Assume that the 124 two-dimensional MR images are arranged in order along the z-axis as shown in Figure 5. The ROIs in this subsection are: the left cerebral hemisphere(LCH for short), the right cerebral hemisphere(RCH), the cerebellum(CB) and the brain stem(BS). For a given 3D MR image we can obtain the whole brain region in Section 2. For the obtained brain data, assume the center of gravity of the brain region as the origin and its coordinate system is shown in Figure 5.

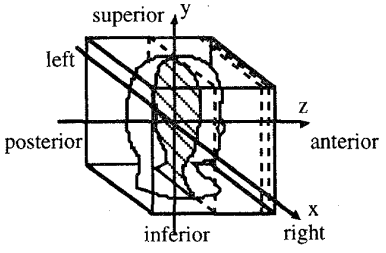

Figure 5 Coordinate system.

(i) Location knowledge: For each axis of x, y and z, Table 2 tabulates which location every ROI belongs to. In it, N, Ze and P express Negative, Zero and Positive membership functions, respectively, in Figure 6. The horizontal axis corresponds to arrows, x, y, or z, in Figure 5. The membership functions VH, H, L and VL are shown in Figure 6.

Table 2 A knowledge table on the ROIs.

	ROI	μ_{LCH}	μ_{RCH}	μ_{CB}	μ_{BS}
X	N	VH	VL	VH	VL
	Ze	L	H	VH	VH
	P	VL	VH	VH	VL
Y	N	L	L	VH	VH
	Ze	H	H	H	H
	P	VH	VH	VH	VL
Z	N	VH	VH	VH	VL
	Ze	VH	VH	H	VH
	P	VH	VH	VH	L

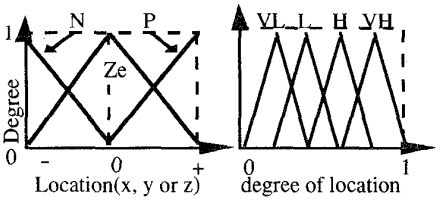

Figure 6 The membership functions.

The notation μ_X denotes the membership function of the ROI X. From Table 2, the rules of x-axis of LCH is derived:
If x=N(left) then $\mu_{LCH} = VH$,
else if x=Ze(middle) then $\mu_{LCH} = L$,
else if x=P(right) then $\mu_{LCH} = VL$.
For a given voxel with coordinate (a, b ,c), a fuzzy inference result, U_{LCH}, is obtained via a min-max inference,

$$U_{LCH}(a) = [a \wedge N \wedge VH] \vee [a \wedge Ze \wedge L] \vee [a \wedge P \wedge VL].$$

The center of gravity, $\mu_{LCH}(a)$, of U_{LCH} is obtained. We can also obtain $\mu_{RCH}(a)$, $\mu_{CB}(a)$ and $\mu_{BS}(a)$ for a of (a, b, c). Similarly, we can obtain the values, $\mu_{LCH}(b)$ and $\mu_{LCH}(c)$, for b and c of (a, b, c), respectively. Finally, we determine a degree $\mu_{LCH}(a,b,c) = \mu_{LCH}(a) \wedge \mu_{LCH}(b) \wedge \mu_{LCH}(c)$, for the voxel as the degree for the left cerebral hemisphere. Similarly, the degrees $\mu_{RCH}(a,b,c)$, $\mu_{CB}(a,b,c)$ and $\mu_{BS}(a,b,c)$, for the other ROIs are also obtained. Thus we can determine a set $[\mu_{LCH}(a,b,c), \mu_{RCH}(a,b,c), \mu_{CB}(a,b,c), \mu_{BS}(a,b,c)]$ for every voxel.

For the obtained set,
IF only one degree, μ_P, of the set is lager than 0.5, we determine the voxel belongs to the ROI "p".
ELSE, we employ the fuzzy inferences of (ii) and (iii)

(ii) Boundary knowledge

a) Proximity: The difference between μ_P and μ_Q can serve an indicator of the boundary surface. The degree $\mu^{Pr}_{1}(P, Q)$ is defined as $(1-|\mu_P - \mu_Q|)\times\mu_P\times\mu_Q$.

b) Euclidean distance: There exists the narrow part between adjacent ROIs. We calculate the Euclidean distance, ε, from the voxel to the outside of the brain region (background region). The voxel closer to the boundary surface implies the higher possibility of boundary. The notation μ^{E}_{B} denotes the degree of the boundary, then,

If the distance ε is L then μ^{E}_{B} is HI,
else if the distance ε is M then μ^{E}_{B} is MI,
else if the distance ε is H then μ^{E}_{B} is LO.

The center of gravity, μ^{E}_{2}, of the obtained inference result is a degree of the boundary surface. The membership functions L, M, H and HI, MI, LO are shown in Figure 7.

(iii) Intensity knowledge : The boundary surface mainly consists of the gray matter. The notation μ_B^I denotes a boundary information on intensity on the gray matter. Then,

If the intensity is L then μ_B^I is HI,

else if the intensity is M then μ_B^I is MI,

else if the intensity is H then μ_B^I is LO.

The center of gravity, μ_3^I, of the inference result is a degree of boundary surface with respect to intensity.

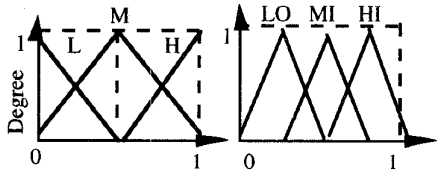

Figure 7 L, M, H and HI, MI and LO membership functions.

Table 2 The weight table.

Pair i	ROI P	ROI Q	ω_i^α	ω_i^β	ω_i^γ
1	LCH	RCH	1	1	0
2	LCH	CB	0	1	1
3	LCH	BS	1	1	0
4	RCH	CB	0	1	1
5	RCH	BS	1	1	0
6	CB	BS	1	1	0

Combine of three inference results by

$$\mu_t = \max_{\{\text{pair } i : i=1..6\}} \{\omega_i^\alpha \mu_1^{Pr}(P,Q) + \omega_i^\beta \mu_2^E + \omega_i^\gamma \mu_3^I\} .$$

Since $\mu_1^P(P,Q) = \mu_1^P(Q,P)$, we can consider all cases with Table 2. Thus obtaining a total degree from all inference results. Finally, we construct the voxels on the region growing by including smaller μ_t as the ROI.

Results: We applied the method to 36 MR voxel data. Our method can segment all voxel data with average error ratio 2.7 %. It required about three minutes on each MR voxel data on IRIS Indigo2 (IRIX 5.3, 150Mz, 128M).

3.2.2 Human Foot CT images

This subsection is to segment the whole bone region into their ossa. The CT images are obtained from Somatom Plus-S CT scanner (Siemens Erlangen, Germany). Field of view was 220mm. Matrix was 512 by 512. This generated 64, 3.44mm-thick, contiguous section images; giving voxel dimensions of $0.43\times0.43\times3.44\text{mm}^3$. We construct the voxel data consisted of $64\times512\times512$ voxels. The intensity ranged between 0 and 2048. First, we extract the whole bone region based on the region growing algorithm with threshold 1180.

(i) Boundary knowledge: The voxel can be closer to the narrow part as the Euclidean distance becomes smaller. We can then derive the following rules in the similar way in the case of Sect. 3.2.1. The notation μ^B denotes a degree of boundary surface for the segmentation. Then,

If the distance $\mathcal{E}$ is L then μ^B is HI, else if $\mathcal{E}$ is M then μ^B is MI, else $\mathcal{E}$ is H then μ^B is LO.

The center of gravity, μ_1^E, of the obtained inference result is a degree of the boundary surface.

(ii) Intensity knowledge : The intensity of bone edges has high. Therefore,

If the intensity is L then μ^B is LO, else if the intensity is M then μ^B is MI, else the intensity is H then μ^B is HI.

The center of gravity, μ_2^I, of the obtained inference result is a degree of boundary surface with respect to intensity.

(iii) Joint knowledge : Figure 8 shows the joint part intensity distribution. A value of J=(lmax-min)(rmax-min) can indicate the joint knowledge. The notation μ^J denotes a degree of joint knowledge of bones. Then,

If the J is L then μ^J is LO, else if J is M then μ^J is MI,

else J is H then μ^J is HI.

The center of gravity, μ_3^J, of the obtained inference result is a degree of Joint knowledge.

Combine of three inference results by

$$\mu_t = \frac{\mu_1^E + \mu_2^I + \mu_3^J}{3} .$$

Thus we obtain a total degree from all inference results. Finally, we construct the voxels on the region growing by including smaller μ_t as the ROI.

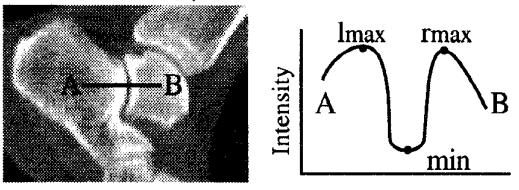

Figure 8 Joint part image and the intensity distribution.

Results: We can correctly segment five images of seven CT data sets. A comparison with genuine ROIs from the viewpoint of anatomy shows that our method precisely segmented them. It required about ten minutes on each 3D human foot CT voxel data on the IRIS Indigo2.

4. FUZZY CLUSTER IDENTIFICATION

4.1. Preliminaries

We obtained the MR angiography images from the MRI scanner. The image acquisition method was 3D TOF Angiography with TR = 61 msec and TE = 3 msec. Field of View (FOV) was 120 mm. Matrix was 256 by 256. Thickness of the slice was 0.8 mm. The dimension of given voxel was $0.47 \times 0.47 \times 0.8\ \text{mm}^3$. In our work, the feature images appear and treated as intensity images. The intensity of all intracranial structure ranged between 0 and 4096. We construct the clusters with continuos hierarchy

clustering. We define a similarity measure between two clusters with the within-class variance and the between-class variance. Our hierarchy clustering is : Consider the number of clusters be equal to the number of voxels; For all combination of two clusters connecting with each other, we calculate the similarity measure; Combine two clusters with minimum similarity measure into one cluster. In the result we obtain hundreds of clusters.

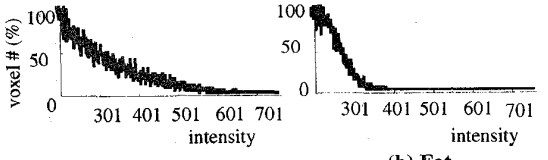

(a) Blood vessel. **(b) Fat**

Figure 9 Typical intensity histogram.

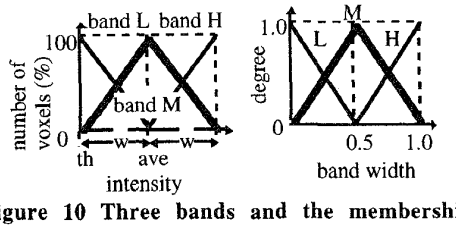

Figure 10 Three bands and the membership functions.

4. 2 Cluster Identification

The clusters obtained in Section 4.1 has coherent intensity distributions, that is, the blood vessel region consists of many voxels with high intensity and fat region consists of many voxels with low intensity. These intensity distributions overlap each other. To recognize intensity distribution of the cluster, we can make a model expressing the coherent intensity distributions in fuzzy languages. Typical intensity of the blood vessel and the fat are shown in Figure 9. Whole range of intensity distribution is divided into three bands, "band L," "band M" and "band H", and each of them can be represented by fuzzy languages, "Low, L" "Middle, M" and "High, H", as shown in Figure 10. In the case of the blood vessel, the fuzzy model of intensity distribution is expressed by $Model_{blood}$(band L, band M, band H) = (don't care, middle, high). In the case of the fat, $Model_{fat}$ = (high, middle, low). For an interested cluster X=(X1, X2, X3), we make up the intensity distribution and we calculate the minimum among three minimums for all bands. We classify the clusters into either the blood vessels or other tissues by picking up larger one of the minimums. Thus, we can identify all clusters to be blood vessel or fat.

Results: We apply our method to some 3D TOF MRA data. Our cluster identification successfully recognizes every cluster. The results show that our method can successfully segment the blood vessel region.

5. CONCLUSIONS

This paper introduced fuzzy logic approaches to segment human brain MR, foot CT and MRA images. Figure 11 summarized these segmentation results. Thus, fuzzy logic can provide powerful tools to manipulate human knowledge.

Acknowledgment

Research supported in part by Tateishi Science and Technology Foundation, Ishikawa Hospital Grant and the BISC Program of UC Berkeley.

Reference

[1] J. K. Udupa and G. T. Herman: 3D Imaging in Medicine, CRC Press, Inc. (1991).

[2] S. K. Pal : Fuzziness, Image Information and Scene Analysis, in R. R. Yager and L. A. Zadeh (Eds.) An Introduction to Fuzzy Logic Applications in Intelligent Systems, Kluwer Academic Pub. pp.147-183, 1992

[3] L. O. Hall, A. M. Besaid, et al, "A comparison of neural network and fuzzy clustering techniques in segmenting magnetic resonance images of the brain," IEEE Trans. on Neural Networks, vol. 3, no. 5, pp. 672-682 (1992).

[4] A. Namasivayam and L. O. Hall: "The use of Fuzzy Rules in Classification of Normal Human Bran Tissues," IEEE Proc. of North American Fuzzy Information Processing Society, pp. 157-162 (1995).

[5] I. Bloch: "Information Combination Operators for Data Fusion: A Comparative Review with Classification," IEEE Trans. SMC, Part A, vol. 26, pp. 52-67 (1996).

[6] I. Bloch and H. Maitre: "Fuzzy Distance and Image Processing," ACM Symposium on Applied Computing, pp. 570-574 (1995).

[7]S. Kobashi, N. Kamiura and Y. Hata, "Fuzzy Information Granulation on Segmentation of Human Brain MR Images," Journal of Japan Society for Fuzzy Theory and Systems, vol. 10, no. 1, pp. 117-125, Feb. 1998.

[8] S. Kobashi, N. Kamiura , Y. Hata and M. Ishikawa, "Automatic robust threshold finding aided by fuzzy information granulation," Proc. of IEEE 1997 Int. Conf. on Image Processing, pp. 711-714 Oct. 1997

[9] Y.Hata, S.Hirano and N.Kamiura,"Image Granulation Based on Fuzzy Inference", Proc. of 1998 Conference of the North America Fuzzy Information Processing Society-NAFIPS, 1998 (in press)

[10] Y. Hata, S. Kobashi, N. Kamiura and M. Ishikawa, "Fuzzy Logic Approach to 3D Magnetic Resonance Image Segmentation," Information Processing in Medical Imaging, Lecture Notes in Comp. Sci., Vol. 1230, pp. 387-392, Jun. 1997.

[11] L. A. Zadeh : "Toward a theory of fuzzy information granulation and its centrality in human reasoning and fuzzy logic", Fuzzy Sets and Systems, 90, pp.111-127 (1997)

[12] L. A. Zadeh: "Fuzzy sets and Applications," John Wiley and Sons, Inc. (1987).

[13] A. Kandel: "Fuzzy Expert Systems," CRC Press, Inc. (1992).

[14] W. Pedrycz: "Fuzzy Control And Fuzzy Systems, "Research Studies Press Ltd. (1993).

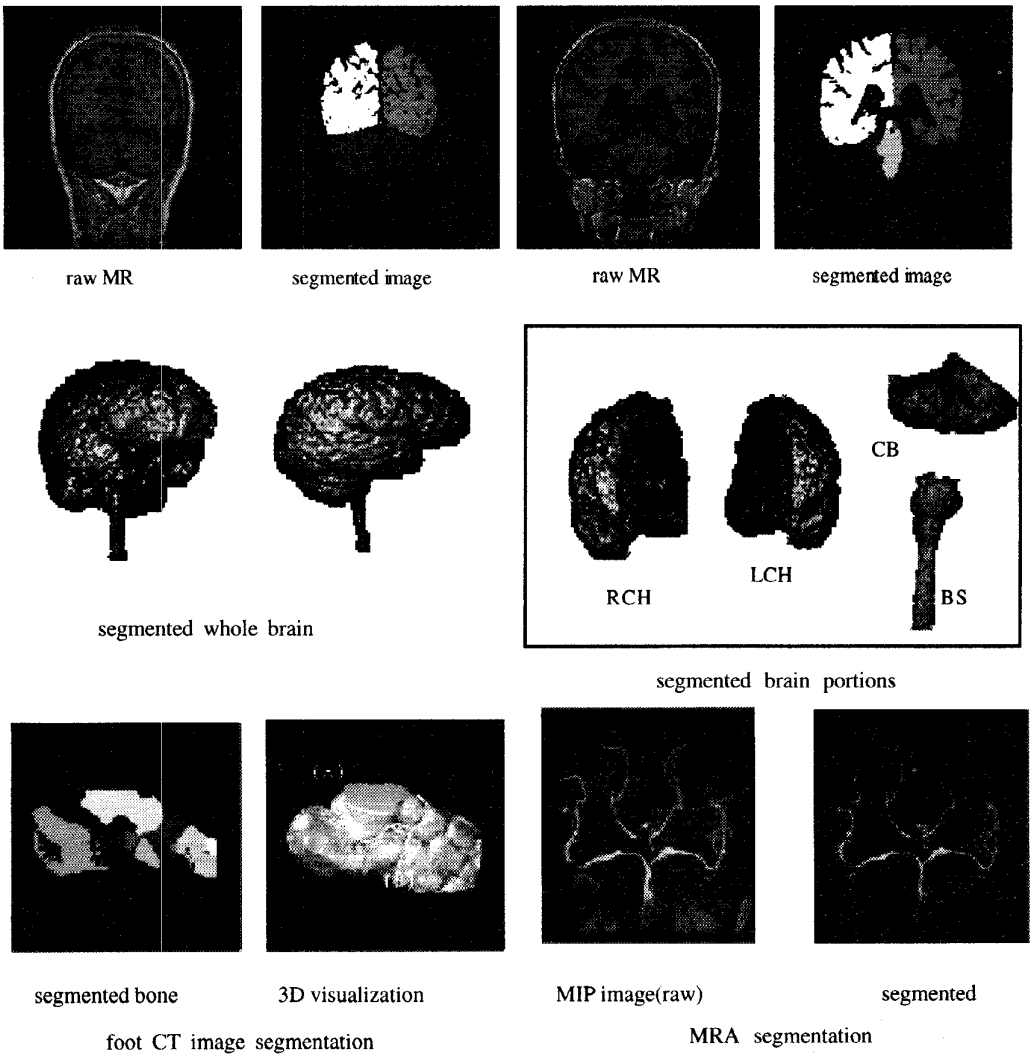

Figure 11 Examples of segmented images.